Combustion and Flame 213 (2020) 302–313

Contents lists available at ScienceDirect

Combustion and Flame

journal homepage: www.elsevier.com/locate/combustflame

Conversion of acenaphthalene to phenalene via methylation: A theoretical study

Denis P. Porfiriev[a,b], Valeriy N. Azyazov[a,b], Alexander M. Mebel[a,c,*]

[a] Samara National Research University, Samara 443086, Russia
[b] Lebedev Physical Institute, Samara 443011, Russia
[c] Department of Chemistry and Biochemistry, Florida International University, Miami, FL 33199, USA

ARTICLE INFO

Article history:
Received 1 July 2019
Revised 14 August 2019
Accepted 22 November 2019
Available online 19 December 2019

Keywords:
Phenalene
Phenalenyl radical
Reaction mechanism
Rate constant
Potential energy surface
RRKM – Master Equation theoretical approach

ABSTRACT

Ab initio calculations of the $C_{13}H_{10}$ and $C_{13}H_9$ potential energy surfaces related to the reaction of 1-acenaphthyl and methyl radicals and secondary isomerization of $C_{13}H_9$ primary radical products have been performed at the chemically accurate G3(MP2,CC)//B3LYP/6-311G** level of theory to unravel the mechanism of conversion of acenaphthalene to phenalene or phenalenyl radical + H. The computed energetics and molecular parameters were utilized in Rice-Ramsperger-Kassel-Marcus Master Equation (RRKM-ME) calculations of reaction rate constants and relative product yields. The 1-acenaphthyl + CH_3 reaction is predicted to proceed by a fast radical-radical recombination mechanism and to predominantly produce collisionally stabilized 1-methylacenaphthalene B1 or a $C_{13}H_9$ benzylic radical A1 + H with exothermicities of 106.8 and 25.2 kcal/mol, respectively. The A1 + H channel is preferable at higher temperatures, whereas the stabilization of 1-methylacenaphthalene is favored at higher pressures. The radical A1 can nearly irreversibly interconvert to phenalenyl radical AP via a 22.7 kcal/mol exothermic isomerization process involving formal insertion of the CH_2 group into a C–C bond of the five-member ring leading to the expansion of this ring to a six-member ring. The rate constants for the H addition reaction to phenalenyl radical to form phenalene and the reverse H loss from phenalene were also computed and the strength of the weakest C–H bond in the CH_2 group of phenalene is evaluated as 62.2 kcal/mol. The analysis of the reaction kinetics allowed us to deduce a mechanism for the conversion of 1-acenaphthyl radical to phenalene or phenalenyl radical + H via methylation involving the formation of A1 via a well-skipping channel or stabilization and dissociation of (or H abstraction from) B1 followed by isomerization of A1 to phenalenyl AP, which can add an H atom producing phenalene. Rate constants for the significant elementary reactions are fitted to modified Arrhenius expressions and are proposed for kinetic modeling of the expansion of a five-member ring on a zigzag edge of PAH to a six-member ring by methylation.

1. Introduction

Ever-growing pressure of environmental changes and technical regulations requires continuous improvement of power units, especially design of cleaner combustion engines. Despite the long way from phenomenological observation to quantitative modeling, there are still many fundamental questions to be answered in order to unravel basic chemical mechanisms driving combustion processes and the emission of environmental pollutants. One of such key problems is the polycyclic aromatic hydrocarbons (PAHs) growth and soot formation. The formation and growth mechanisms of PAH in combustion involve a large variety of reactions between different molecules and radicals formed from fuel pyrolysis and oxidation in distinct isomeric forms [1,2] and are consequently extremely complex. Kinetic models have been developed for the PAH growth [1–22], but the data on the mechanisms and reliable and accurate rate constants of the key elementary chemical reactions involved in these processes are often unavailable, especially for a broad range of temperatures and pressures relevant to combustion conditions. This gap in knowledge calls for predictive theoretical calculations of the rate constants and product branching ratios based on the first physical principles. The widely accepted approach to tackle PAHs formation and enlargement is the Hydrogen-Abstraction/Acetylene-Addition (HACA) mechanism, proposed by Frenklach and co-workers [11]. However, the HACA mechanism cannot provide pathways fast enough to properly explain production of benzenoid tricyclic PAHs phenanthrene and anthracene containing all six-member rings under typical combustion conditions. For instance, both theoretical calculations [23] and

* Corresponding author at: Department of Chemistry and Biochemistry, Florida International University, Miami, FL 33199, USA.
E-mail address: mebela@fiu.edu (A.M. Mebel).

https://doi.org/10.1016/j.combustflame.2019.11.038
0010-2180/

experimental measurements in a pyrolytic reactor at 1200±100 K [24] for the reaction of 1-naphthyl radical with acetylene show preferable formation of acenaphthalene meaning that PAH expansion on a zigzag edge via HACA leads to the formation of an extra five-member ring rather than a six-member ring. As we systematically consider various pathways of PAH growth [25–27], a possible mechanism for the conversion of such five-member ring on an edge of a PAH molecule to a six-member ring needs to be addressed. Another motivation for the present investigation stems from potential importance of five-member rings for the whole process of soot growth/oxidation. Accumulation of such rings embedded in the aromatic edge was suggested, from the site-resolved modeling, to be the cause for the decrease in the oxidation rate [28,29]. Schulz et al. [30] demonstrated using high-resolution atomic force microscopy that at the early stages of soot formation there is significant presence of five-member rings as opposed to the purely benzenoid aromatic compounds. The five-member rings on PAH edges can be either oxidized or expand to six-member rings via reactions with another hydrocarbon or a radical.

The five- to six-member ring expansion process has been now well established for an isolated five-member ring, a cyclopentadienyl radical C_5H_5 [31–33], and for a five-member ring attached to benzene, as in a 1-indenyl radical [26,34,35]. In both systems, the ring expansion can readily occur by methylation, i.e., via the addition of a CH_3 radical eventually leading to the formation of benzene and naphthalene, respectively. This conclusion was made from ab initio calculations of the potential energy surfaces (PESs) for these reactions combined with Rice-Ramsperger-Kassel-Marcus Master Equation (RRKM-ME) calculations of phenomenological rate constants and product branching ratios depending on temperature and pressure. Moreover, the formation of naphthalene through recombination of indenyl and methyl radicals was recently confirmed by experimental measurements in a pyrolytic microreactor with product detection utilizing photoionization mass spectrometry (PIMS) [35]. Taking these reactions into account allowed us to propose a mechanism of PAH growth, which involves H abstractions, alternating additions of methyl radical and acetylene, and H-assisted isomerizations beginning from cyclopentadienyl or benzene [26]:

$$C_5H_5 + CH_3 \rightarrow C_5H_5CH_2 + H$$

$$C_5H_5CH_2 \rightarrow C_6H_6\ (\text{fulvene/benzene}) + H$$

$$C_6H_6\ (\text{fulvene}) + H \rightarrow C_6H_6\ (\text{benzene}) + H$$

$$C_6H_6\ (\text{benzene}) + H \rightarrow C_6H_5\ (\text{phenyl}) + H_2$$

$$C_6H_5 + CH_3 \rightarrow C_6H_5CH_3\ (\text{toluene}) \rightarrow C_6H_5CH_2\ (\text{benzyl}) + H$$

$$\text{benzyl} + C_2H_2 \rightarrow C_9H_8\ (\text{indene}) + H$$

$$\text{indene} + H \rightarrow C_9H_7\ (\text{indenyl}) + H_2$$

$$\text{indenyl} + CH_3 \rightarrow C_{10}H_9\ (\text{1-/2-methylindenyl}) + H$$

$$\text{1-2-/methylindenyl} \rightarrow C_{10}H_8\ (\text{benzofulvene/naphthalene}) + H$$

$$C_{10}H_8\ (\text{benzofulvene}) + H \rightarrow C_{10}H_8\ (\text{naphthalene}) + H$$

While this mechanism can reflect a prototype PAH growth step adding an extra six-member ring, it cannot be adopted directly when a five-member ring is located on a zigzag edge. The simplest example of such geometry is the acenaphthalene molecule, which is considered as the first significant island of stability "pulling" the HACA sequence forward [36]. Here, the 1-acenaphthyl radical, which can be formed by abstraction of an H atom linked to the five-member ring, can react with CH_3 and the expansion of the five-member ring if happens would then produce a benzenoid three-ring phenalene molecule, $C_{13}H_{10}$. However, the mechanism and kinetics of this reaction has never been theoretically studied before, to our knowledge.

A related mechanism involving methyl radical additions alternating with dehydrogenation was proposed earlier by Shukla et al. and was called methyl addition/cyclization (MAC) [37]. The authors deduced this mechanism from the kinetic analysis of mass spectra of the gas-phase products in the pyrolysis of toluene and toluene/acetone mixtures. Shukla et al. concluded that MAC promotes sequential growth of hexagonal networks of sp^2 carbons from all fusing sites of a PAH and is responsible for the expansion of cyclopentafused PAH to benzenoid PAH. Although Shukla et al. have noted that the MAC mechanism is not as efficient as HACA, MAC plays a special role in the conversion of five-member rings to six-member rings. In particular, based on the observed mass spectra, Shukla et al. included the transformation of acenaphthalene ($m/z = 154$) to phenalene ($m/z = 166$) via H abstraction and methyl addition into their MAC mechanism.

Phenalene is also interesting for another reason – the C–H bond in the CH_2 group is rather weak and hence, one of the H atoms can be readily abstracted (or eliminated via thermal unimolecular decomposition of phenalene) to form a resonantly stabilized radical (RSFR) phenalenyl, $C_{13}H_9$. Phenalenyl and its higher homologues were recently speculated to play a critical role in the PAH nucleation process [38] representing a kinetic bottleneck in the growth of soot particles. Also, Wornat and co-workers deduced an important role of phenalenyl and higher-ring number phenalenyl-type radicals in the formation of large benzenoid PAHs via their reactions with the C_2–C_4 1-alkenes and phenalenyl/arylmethyl recombinations in the supercritical pyrolysis of n-decane and 1-octene and predicted these PAH-growth pathways to have widespread applicability to larger PAH [39,40]. Therefore, rate constants for the formation of phenalene and phenalenyl are essential not only for the PAH growth kinetic models but also for those for soot formation. In the present paper, we study the PES for the reaction of 1-acenaphthyl with methyl radical to account for the transformation mechanism of a five-member ring on a zigzag PAH edge into a six-member ring leading to a phenalene-like structure. This is followed by RRKM-ME calculations of the rate constants to be included in the kinetic models.

2. Theoretical methods

Geometries of the reactants, products, transition states, and reaction intermediates have been optimized using the density functional B3LYP level of theory [41,42] with the 6–311G** basis set. Vibrational frequencies were computed at the same B3LYP/6–311G** level of theory to confirm the nature of the optimized stationary points, to evaluate zero-point vibrational energy (ZPE) corrections. All B3LYP calculations were performed employing the Gaussian 09 program package [43]. Single-point G3(MP2,CC) calculations were run at the B3LYP optimized geometries and the total energies were determined as follows [44,45]:

$$E_0[\text{G3(MP2,CC)}] = E[\text{CCSD(T)/6–311G}^{**}] + \Delta E_{\text{MP2}} + E(\text{ZPE})$$

Here, ΔE_{MP2} is a basis set correction, $\Delta E_{\text{MP2}} = E[\text{MP2/G3Large}] - E[\text{MP2/6–311G}^{**}]$, and E(ZPE) is the zero-point energy. Restricted RHF-RCCSD(T) and unrestricted UMP2 energies were used for open-shell species; RHF-RCCSD(T) stands for partially spin-adapted open-shell coupled cluster singles and doubles theory augmented with a perturbation correction for triple excitations starting from molecular orbitals obtained from restricted open shell Hartree−Fock calculations. For coupled cluster calculations,

the degree of a multireference character of wave functions was monitored through T1 diagnostics. The predicted accuracy of G3(MP2,CC) relative energies lies within 1–2 kcal/mol [44,45].

Temperature- and pressure-dependent rate constants for the reactions considered were evaluated within the framework of the RRKM-ME approach [46–48]. The MESS code [49,50] was used for the rate constant calculations in the temperature range of 300–2500 K and in the pressure range of 0.01–100 atm. The rigid rotor-harmonic oscillator approximation (RRHO) was employed in partition function calculations. "Soft" vibrational modes, which can be characterized as intramolecular rotations and have low vibrational frequencies, were treated as hindered rotors. The internal rotational potentials for the hindered rotors were evaluated using B3LYP/6-31G* calculations. We used collision parameters for RRKM-ME calculations derived in the literature for similar systems; the Lennard-Jones parameters ε and σ for hydrocarbons were taken from Wang and Frenklach [51] and those for N_2 bath gas from Vishnyakov et al. [52,53] Collisional energy transfer in ME was described using the "exponential down" model [54], where the temperature dependence of the range parameter α for the deactivating wing of the energy transfer function is expressed as $\alpha(T)=\alpha_{300}(T/300\,\mathrm{K})^n$, with $n=0.62$ and $\alpha_{300}=424\,\mathrm{cm}^{-1}$, derived by Jasper from classical trajectory calculations [55] and used earlier by us in the studies of the systems of similar sizes, $C_8H_7+C_2H_2$ [25], indenyl $+CH_3$ [26], $C_{10}H_7+C_2H_2$ and $C_{14}H_9+C_2H_2$ [56]. We have also repeated the RRKM calculations with $n=0.85$ and $\alpha_{300}=247\,\mathrm{cm}^{-1}$ proposed by Jasper and Miller as 'universal' values for hydrocarbons [55] and with intermediate values of $n=0.70$ and $\alpha_{300}=333\,\mathrm{cm}^{-1}$. A comparison of the results showed that deviations in the computed rate constants did not exceed a factor of 2, i.e., kinetic accuracy. In fact, for most accurate calculations, the collisional energy transfer parameters can be considered as empirical and be adjusted if experimental data on the pressure dependence are available, which is not the case for this system.

To tackle barrierless reactions of CH_3- or H-elimination/addition to a radical site, we used phase space theory [57]. For that treatment, we chose the rate constants for $C_6H_5+CH_3$ [58] and recombination of hydrocarbon radicals with an H-atom [59] as references because they seem to be the best available ones due to similar delocalization of electron density and position of the radical sites. For instance, both phenyl and acenaphthyl are aromatic σ radicals and the strengths of the forming C–C bonds are similar, 104 and 107 kcal/mol, respectively, where the value for acenaphthyl was computed here and that for phenyl was obtained in [58] at a similar CCSD(T)/aug-cc-pvdz//B3LYP/6–31G* level of theory. Thus, the $C_6H_5+CH_3$ system has the largest similarity with acenaphthyl $+CH_3$ among all systems, for which high-pressure rate constants were computed using variable transition state transition state theory (VRC-TST), which is the most accurate theoretical approach available up-to-date. While we cannot quantify the uncertainty of this assumption, a comparison of the $C_5H_5+CH_3$ [33] and $C_6H_5+CH_3$ [58] high pressure limit rate constants show that they differ by a factor of 2 or less at combustion temperatures of 1000 K and above indicating that the values for barrierless reactions of CH_3 with cyclic hydrocarbon radicals vary in a relatively narrow range under such conditions. Unfortunately, robust VRC-TST calculations for $C_{12}H_7+CH_3$ using a reliable CASPT2 potential with an appropriate active space are currently not feasible. Potential power exponents and prefactors in phase space theory calculations were fit to match the high-pressure limit (HP) rate constants to the reference ones multiplied by scaling factors introduced to account for the differences in the reaction path degeneracies. For instance, for the initial recombination of 1-acenaphthyl and methyl radicals, the $C_6H_5+CH_3$ HP rate constant [58] was taken as a target without scaling. For A1 + H → B1, the rate constant for the R1 + H → $C_5H_5CH_3$-1 reaction from the study of the $C_5H_5+CH_3$ reaction [33] was also used without scaling, for A1 + H → B2, we employed the rate constant for the H-addition to an *ortho* position in benzyl radical multiplied by a factor of 1/2 [59], and for AP + H → BP we utilized the rate constant for H-addition to cyclopentadienyl with a scaling factor of 6/5 [59]. The phase space theory HP rate constants were combined with regular RRKM rate constants in Master Equation calculations of the pressure dependence by the MESS package.

The similar ab initio/RRKM-ME approach was earlier used by our group to study various PAH formation and growth reactions (see e.g. [25–27,56]) and its validation vs. available experimental data has generally shown that this method is able to provide kinetic accuracy. Since the comparison with experiment is not possible for the present system, we can only anticipate a similar accuracy here taking into account the additional uncertainty (likely within a factor of 2) due to the use of the $C_6H_5+CH_3$ high pressure limit rate constant to fit that for the entrance $C_{12}H_7+CH_3$ channel.

3. Results and discussion

3.1. Potential energy surfaces

The calculated potential energy diagram is shown in Fig. 1, where the bottom and top parts relate to the $C_{13}H_{10}$ and $C_{13}H_9$ surfaces, respectively. The initial reaction step is a barrierless recombination of 1-acenaphthyl and methyl radicals. It should be noted that the potential well at −106.8 kcal/mol corresponding to the produced closed shell molecule 1-methylacenaphthalene, B1, is much deeper than that for the related reaction of indenyl and methyl radicals, −67.4 kcal/mol [26]. After the initial recombination of the two radicals the reaction can proceed by three possible pathways, two different channels of intramolecular isomerization of the $C_{13}H_{10}$ species and an immediate loss of an H-atom from methyl to form A1 followed by isomerization of $C_{13}H_9$ radicals. The first isomerization pathway to phenalene BP denoted in blue in Fig. 1 begins with an H-shift from the neighboring C atom in the five-member ring to the *ipso* position with respect to CH_3, is followed by a second H-shift from the methyl group back to the *ortho* carbon atom, and leads to the formation of a stable symmetric intermediate B4, in which the CH_2 group bridges two CH groups in the five-member ring. The barrier for the initial step B1 → B3 through a transition state (TS) B1-B3 is 71.6 kcal/mol, however, this rearrangement possesses a low barrier of 4.5 kcal/mol in the backward direction, whereas the next step along this pathway, B3 → B4, requires overcoming a barrier of 10.4 kcal/mol. Thus, the well B3 is metastable and unlikely to be detectable even at low temperatures. Alternatively, the potential well corresponding to B4 is almost as deep as the one for B2 and hence B4 is anticipated to be among collisionally stabilized $C_{13}H_{10}$ reaction products. Effectively, the B1 → B3 → B4 two-step sequence proceeds through a higher barrier of 77.5 kcal/mol at TS B3–B4. The final ring expansion goes through metastable B6 and the barrier at TS B6-BP, 86.8 kcal/mol above B1, which is the highest energy along the B1 → B3 → B4 → B6 → BP channel. B6 was found as a local minimum at the B3LYP level but at the higher G3(MP2,CC)//B3LYP level its energy is 0.2 kcal/mol higher than that of TS B4-B6. The second isomerization pathway denoted in green in Fig. 1 starts with another H-shift B1 → B2 via TS B1-B2 and exhibits a barrier of 70.7 kcal/mol. The B1 → B2 isomerization involves 1,3-H shift from the methyl group to the C atom in the *ortho* position in the five-member ring. The barrier for the reverse H-shift, B2 → B1, is 67.5 kcal/mol. TS B2-B5 for the ensuing ring expansion via insertion of the out-of-ring CH_2 group into the adjacent C–CH_2 bond, B2 → B5, resides even higher in energy, 81.4 kcal/mol relative to B2. Such configuration of the PES should

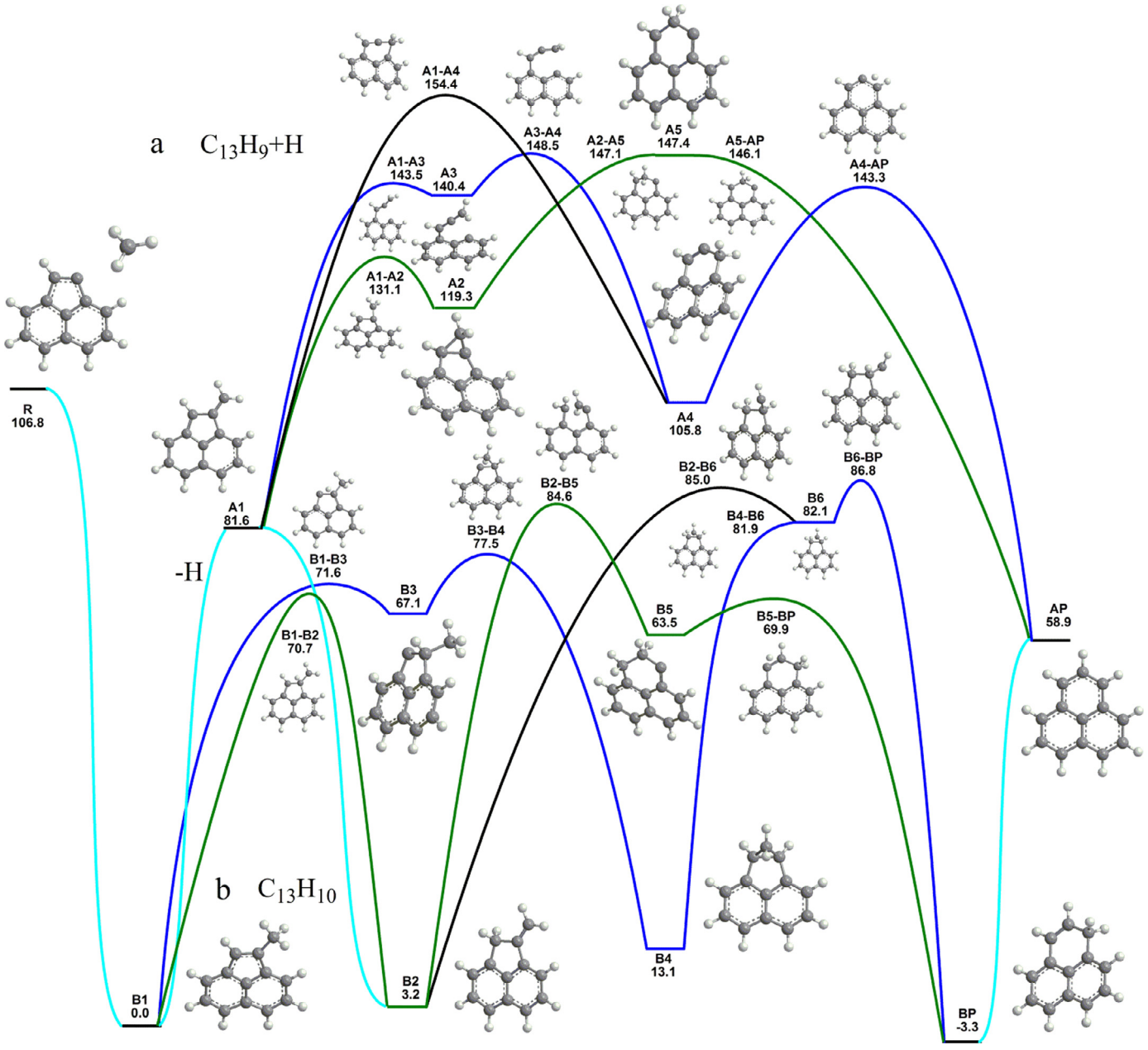

Fig. 1. Potential energy diagram of the 1-acenaphthyl + CH_3 reaction and related reactions on the $C_{13}H_{10}$ and $C_{13}H_9$ PESs calculated at the G3(MP2,CC)//B3LYP/6-311G** level of theory. Relative energies are shown in kcal/mol with respect to the 1-acenaphthyl + CH_3 reactants.

result in significant probability for collisional stabilization of B2, at least at low temperatures and high pressures. The final step towards phenalene along this pathway is an H-shift from the CH_2 group originated from the methyl radical to the bare C atom. The equilibrium between B5 and phenalene, BP, is expected to be shifted toward phenalene due to a low barrier in forward direction, 6.4 kcal/mol, and a high barrier, 73.2 kcal/mol, in the backward direction. Another route from B2 towards BP goes through the metastable B6 intermediate. This path exhibits higher barriers of 81.8 and 85.6 kcal/mol relative to B2 and involves H-shift from the out-of-ring CH_2 group to the *ipso* carbon forming B6 followed by a ring expansion via insertion of the outer CH group into the neighboring C–C bond. In summary, the two competing pathways from the initial recombination complex B1 to phenalene, B1 → B3 → B4 → B6 → BP and B1 → B2 → B5 → BP, have the highest barriers of 86.8 and 84.6 kcal/mol, which are however significantly lower than the energy of chemical activation of B1 produced in the 1-acenapthyl + CH_3 reaction, 106.8 kcal/mol. B1 can also lose an H atom from the methyl group forming $C_{13}H_9$ (A1), with the energy of 81.6 kcal/mol required for this endothermic process to occur. B2 can eliminate an H atom to form A1 as well, whereas H elimination from phenalene BP produces phenalenyl radical AP with an energy loss of 62.2 kcal/mol. Interestingly, earlier calculations of this bond strength at the B3LYP/6-31G* level by Zoellner and Zoellner gave a similar but somewhat higher value of 65.1 kcal/mol [60]. Clearly, the C–H bond in the CH_2 group of phenalene is relatively weak owing to a large resonant stabilization of phenalenyl. All H elimination steps from $C_{13}H_{10}$ to $C_{13}H_9$ do not exhibit exit barriers and the H losses should compete with isomerization of $C_{13}H_{10}$. It is also important to note that all the species on the $C_{13}H_{10}$ PES and the $C_{13}H_9$ + H products, such A1 and AP, have relative energies considerably lower than that of the reactants.

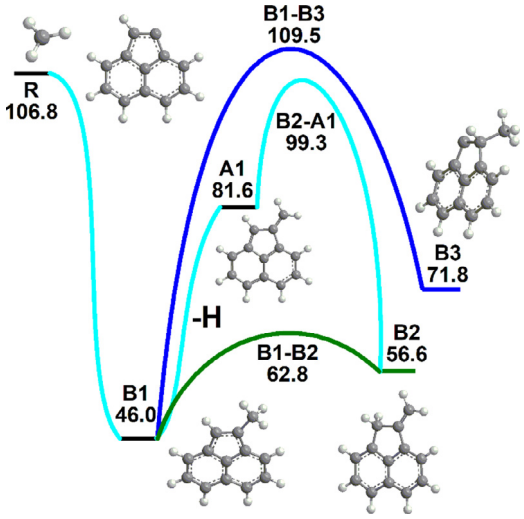

Fig. 2. Potential energy diagram of the 1-acenaphthyl + CH_3 reaction in the triplet electronic state calculated at the G3(MP2,CC)//B3LYP/6-311G** level of theory. Relative energies are shown in kcal/mol with respect to the 1-acenaphthyl + CH_3 reactants.

The rearrangements on the $C_{13}H_9$ PES start from A1 which can undergo expansion of the five-member ring via three different pathways. Direct insertion of the outer CH_2 group into the adjacent C–C bond in the five-membered ring leading to A4 is the most energetically demanding process with a barrier of 72.8 kcal/mol at TS A1-A4. The alternative route to A4 consists of two steps. Ring opening at TS A1-A3 with a barrier of 61.9 kcal/mol in forward direction and only 3.1 kcal/mol in backward direction precedes six-member ring re-closure via a barrier at TS A3-A4 of 8.1 and 42.7 kcal/mol in the forward and backward directions, respectively. Analogously to B3 on the $C_{13}H_{10}$ PES, the intermediate A3 is anticipated to be metastable. The intermediate A4 then forms the most stable $C_{13}H_9$ isomer AP (phenalenyl radical) by H migration from the CH_2 group in the newly formed six-member ring to the neighboring bare C atom featuring a barrier of 37.5 kcal/mol at TS A4-AP. A slightly more energetically favorable ring expansion in A1 also requires two reaction steps. The first one is formation of a three-membered ring with the methylene group CH_2 moving toward the neighboring C atom occurring via a barrier at TS A1-A2, 49.5 kcal/mol in forward and 11.8 kcal/mol in backward directions. The second step is literally ring expansion A2 → A5. The intermediate A5 appears to be metastable according to our calculations since the transition states separating it from A2 and AP located at the B3LYP level of theory appeared to be slightly lower in energy than A5 when the energies were refined at the G3(MP2,CC) level. Thus, the overall process can be described in terms of ring expansion immediately followed by a spontaneous H migration from CH_2 to the adjacent bare C atom. Barriers for $C_{13}H_9$ isomerization are generally significantly lower than those for $C_{13}H_{10}$, for instance, for the A1 → A3 → A4 → AP and A1 → A2 → A5 → AP pathways the highest barriers are 66.9 and 65.8 kcal/mol, respectively.

Both $C_{13}H_{10}$ and $C_{13}H_9$ PESs are connected through H-detachment or attachment. The reactions connecting the two surfaces include B1 ⇆ A1 + H and B2 ⇆ A1 + H, or BP (phenalene) ⇆ AP (phenalenyl) + H. Special attention should be paid to the initial step of the reaction. The energy of the reacting radicals is 106.8 kcal/mol above 1-methylacenaphthalene, B1, whereas the energy required to overcome barriers for isomerization steps or to eliminate an H-atom from the methyl group and to produce A1 structure lies in the 70.7–81.6 kcal/mol range. Therefore, these processes are energetically feasible and their competition is determined by rate constants of the contending reaction channels.

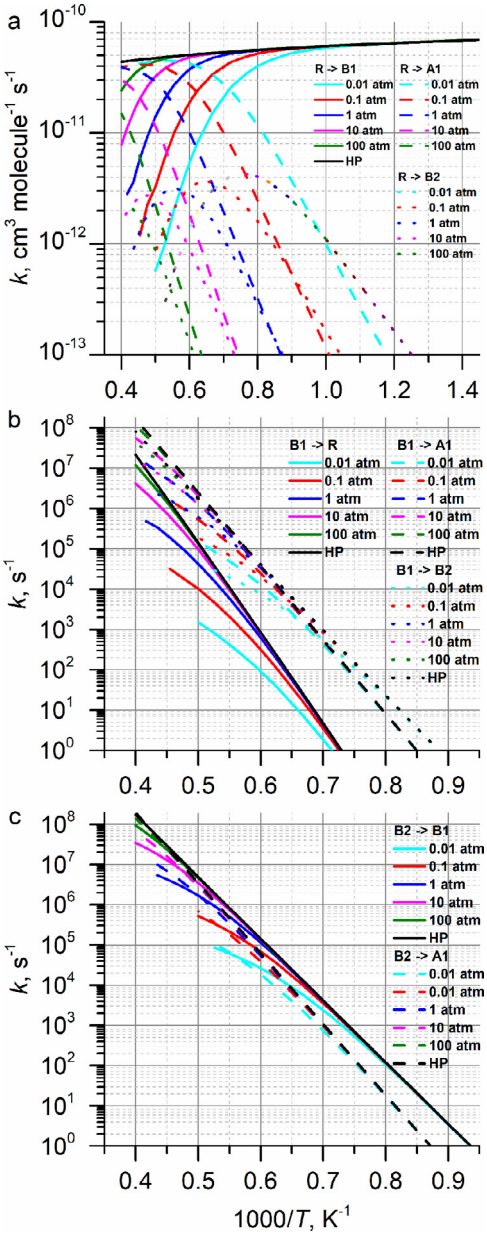

Fig. 3. Rate constants for: (a) 1 - acenaphthyl + methyl → B1 – solid lines, 1 - acenaphthyl + methyl → A1 + H – dashed lines, 1 - acenaphthyl + methyl → B2– dotted lines; (b) B1 → 1 - acenaphthyl + methyl – solid lines, B1 → A1 + H – dashed lines, B1 → B2 – dotted lines, (c) B2 → B1 – solid lines, B2 → A1 + H – dashed lines. Values are shown at various pressures: 0.01 atm – cyan, 0.1 atm – red, 1 atm – blue, 10 atm – magenta, 100 atm – green, high-pressure limit – black. (For interpretation of the references to color in this figure legend, the reader is referred to the web version of this article.)

For comparison, we have also considered the acenaphthyl + CH_3 PES in the first excited triplet electronic state illustrated in Fig. 2. The calculations showed that the initial association step is barrierless like in the singlet state but the resulting triplet complex B1 resides 46.0 kcal/mol above the corresponding triplet intermediate. Triplet B1 can lose a methyl group H atom to produce A1 without an exit barrier or isomerize to triplet B3 via a very high barrier or to triplet B2, which in turn loses an H atom to form A1 via an exit barrier 17.1 kcal/mol above the product. Clearly, the most favorable reaction scenario in the triplet state is $C_{12}H_7 + CH_3$ → triplet B1 → A1 + H. However, since the potential in the entrance channel on the triplet surface is much less attractive than on the singlet

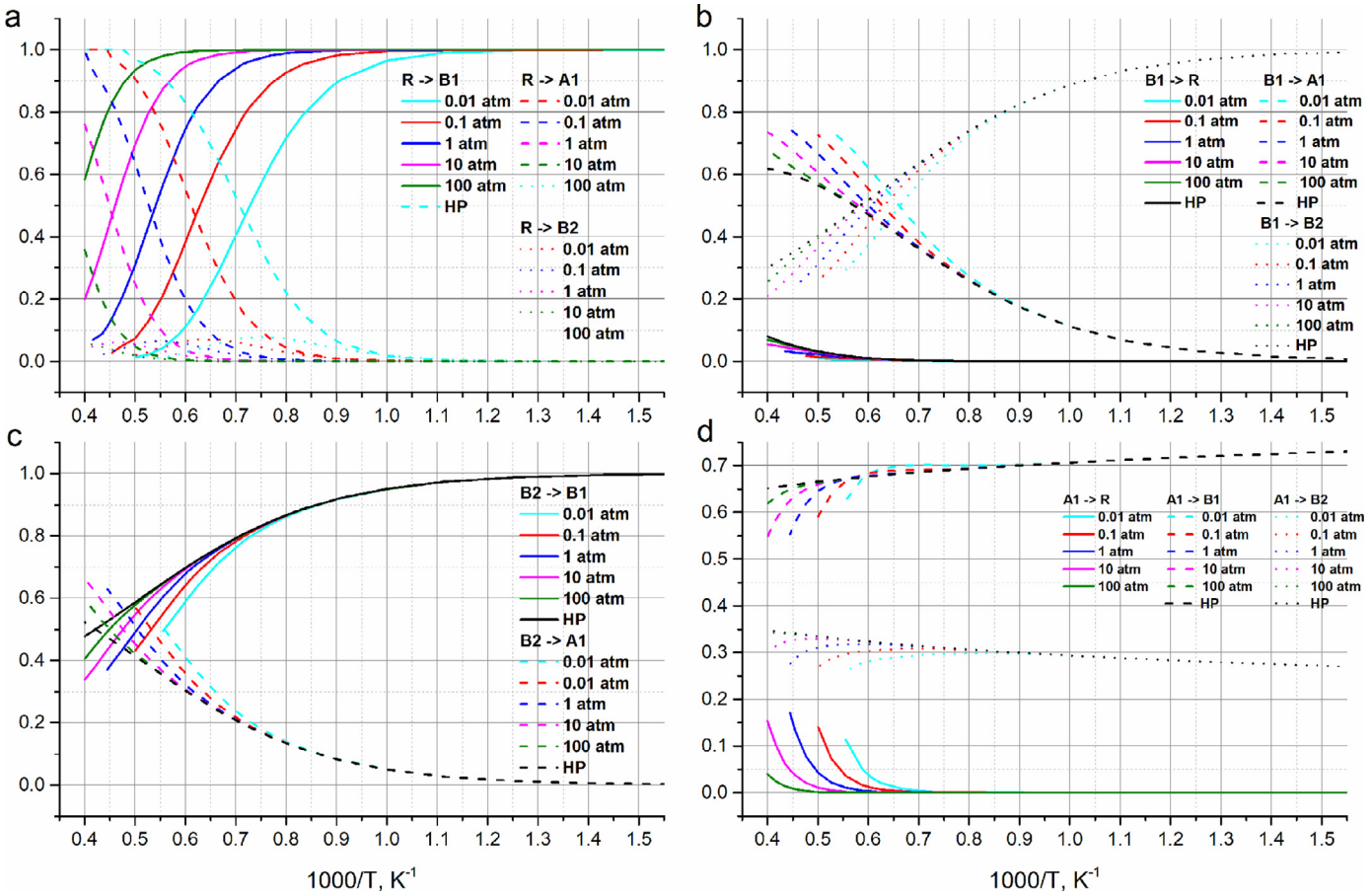

Fig. 4. Branching ratios for the most significant products of the reactions: (a) 1-acenaphthyl + methyl → B1 – solid lines, 1-acenaphthyl + methyl → A1 + H – dashed lines, 1-acenaphthyl + methyl → B2 – dotted lines; (b) B1 → 1-acenaphthyl + methyl – solid lines, B1 → A1 + H – dashed lines, B1 → B2 – dotted lines; (c) B2 → B1 – solid lines, B2 → A1 + H – dashed lines; (d) A1 + H → 1-acenaphthyl + methyl – solid lines, A1 + H → B1 – dashed lines, A1 + H→ B2 – dotted lines. Values are shown at various pressures: 0.01 atm – cyan, 0.1 atm – red, 1 atm – blue, 10 atm – magenta, 100 atm – green, high-pressure limit – black. (For interpretation of the references to color in this figure legend, the reader is referred to the web version of this article.)

surface, we expect that the reaction in the triplet state should be significantly slower than the reaction in the singlet state and hence do not account for the triplet surface in the kinetics calculations.

3.2. Reaction kinetics

Let us first consider the reactions occurring on the $C_{13}H_{10}$ PES. The rate constants for various individual channels of the 1-acenaphthyl + CH_3 reaction and product branching ratios are illustrated in Figs. 3(a) and 4(a), respectively. The RRKM-ME results show that at lower temperatures and higher pressures the reaction is clearly dominated by the formation of the collisionally stabilized complex B1, 1-methylacenaphtalene. Its branching ratio is close to 1 up to 1800 K at the highest pressure of 100 atm, up to 1300 K at 1 atm, but only up to 900 K at the lowest pressure of 0.01 atm. The main competitor at higher temperatures and lower pressures is the well-skipping mechanism forming A1 + H. The branching ratio for this channel overtakes that for collisional stabilization of B1 around 1400 and 1850 K at 0.01 and 1 atm, respectively, but is still lower than the branching ratio of B1 at 2500 K and 100 atm. Collisional stabilization of B2 plays a rather minor role, with its branching ratio never exceeding 10% and reaching its maximal value around 1300 K at 0.01 atm. If the B1 species is thermalized, it mostly undergoes isomerization to the collisionally stabilized intermediate B2 at low temperatures, but at higher temperatures prefers unimolecular decomposition to A1 + H; whereas the contribution of reverse dissociation back to the reactants is rather small (Figs. 3(b) and 4(b)). At the typical combustion temperature of 1500 K, the B1 → B2 and B1 → A1 + H channels compete, with their rate constants being on the range of few 10^3 s^{-1}. Hence, the lifetime of B1 under these conditions is predicted to be on a sub-millisecond scale. In turn, B2 can either isomerize back to B1 or preferably decompose to A1 + H at higher temperatures (Figs. 3(c) and 4(c)). The lifetime of B2 under typical combustion conditions is expected to be few times shorter than that of B1. In summary, the following channels of the 1-acenaphthyl + CH_3 reaction need to be included in a detailed kinetic model:

1-acenaphthyl + CH_3 → A1 + H (well-skipping)

→ B1/B2 (stabilization)

B1 ⇆ B2 (isomerization)

B1/B2 → A1 + H (dissociation)

The results clearly indicate that neither phenalene nor phenalenyl radical can be directly produced in the 1-acenaphthyl + CH_3 reaction. The 1-methylacenaphthalene molecule B1 is much more stable than 1-methylindene, with its decomposition rate constant being few orders of magnitude lower than that for the latter [35]. Therefore, B1 may survive long enough to undergo bimolecular reactive collisions with e.g., H atoms and form A1 via H abstraction from the weakest C–H bond in CH_3. Hence,

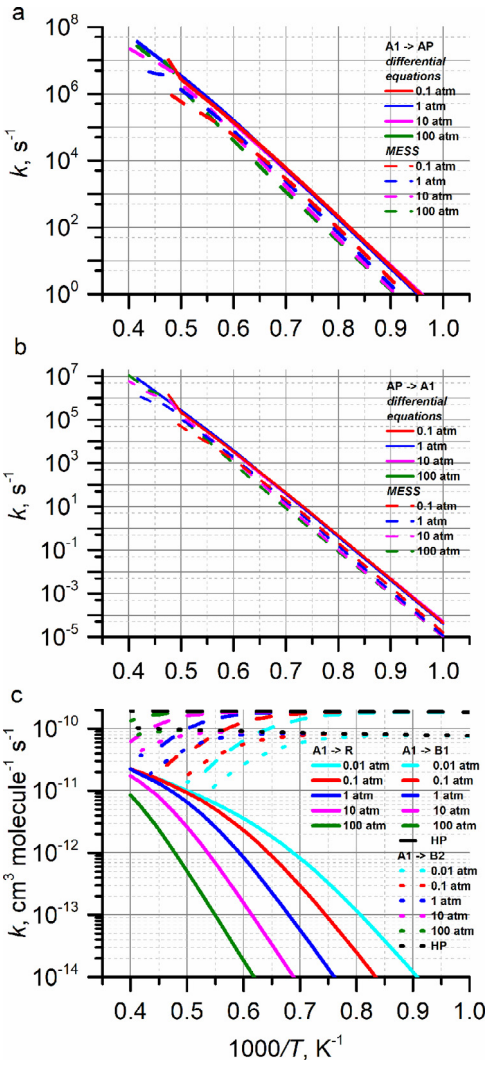

Fig. 5. Rate constants for: (a) A1 → AP: from solving differential equations – solid lines, from RKKM-ME MESS calculations – dashed lines, (b) AP → A1, (c) A1 + H → 1-acenaphthyl + methyl – solid lines, A1 + H → B1 – dashed lines, A1 + H → B2 – dotted lines. Values are shown at various pressures: 0.01 atm – cyan, 0.1 atm – red, 1 atm – blue, 10 atm – magenta, 100 atm – green, high-pressure limit – black. (For interpretation of the references to color in this figure legend, the reader is referred to the web version of this article.)

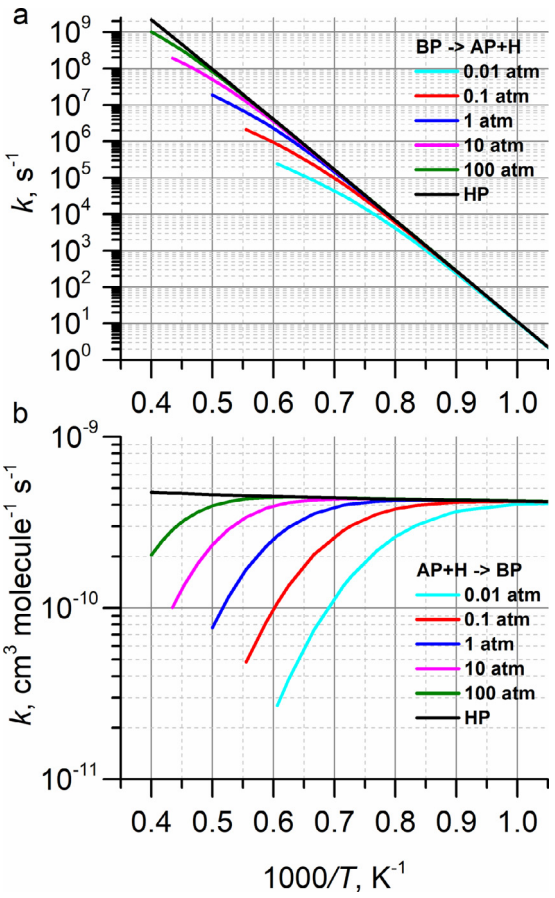

Fig. 6. Rate constants for: (a) BP → AP + H; (b) AP + H → BP. Values are shown at various pressures: 0.01 atm – cyan, 0.1 atm – red, 1 atm – blue, 10 atm – magenta, 100 atm – green, high-pressure limit – black. (For interpretation of the references to color in this figure legend, the reader is referred to the web version of this article.)

it is essential to also consider the kinetics of the $C_{13}H_9$ radical A1. In a unimolecular reaction, A1 can form colissionally stabilized phenalenyl radical AP. The rate constant for this isomerization process is drawn in Fig. 5(a). While the reaction is slow at low combustion temperatures, the rate constant reaches $3–9 \times 10^3$ s^{-1} at 1500 K and rapidly increases to $\sim 10^6$ s^{-1} at 2000 K and exceeds 10^7 s^{-1} at 2500 K. The dependence on pressure is rather week, but pressure determines the highest temperature at which A1 is still stable, i.e., does not equilibrate with AP, 1900, 2200, 2400, and above 2500 K at 0.01, 0.1, 1 and above 10 atm, respectively. The reverse AP → A1 rate constants (Fig. 5(b)) are much lower than those in the forward direction up to the temperatures of 2000 K and hence the isomerization of A1 to phenalenyl radical in that range can be considered practically irreversible. For the temperatures above 2000 K, the reverse isomerization rate constant does not exceed 30% of the forward one. In competition to the unimolecular process, A1 can encounter an H atom and rate constants and product branching ratios for A1 + H are illustrated in Figs. 5(c) and 4(d), respectively. This recombination reaction between two radicals is fast and the finite pressure rate constants decrease with temperature but increase with pressure, because temperature promotes dissociation of the wells B1 and B2 back to A1 + H but pressure, on the contrary, favors collisional stabilization of these wells. The prevailing reaction product is collisionally stabilized B1, but its branching ratio drops to ~50% at the highest temperatures considered, while those of collisionally stabilized B2 and 1-acenaphthyl + CH_3 increase to 30–20%. Therefore, the reverse reactions,

$$A1 + H \rightarrow B1/B2 \text{ (stabilization)}$$

$$\rightarrow \text{1-acenaphthyl} + CH_3$$

should be also included in a detailed kinetic model.

Another bridge between the $C_{13}H_{10}$ and $C_{13}H_9$ stoichiometries connects phenalene and phenalenyl radical, BP ⇆ AP + H. The unimolecular decomposition and recombination rate constants are illustrated in Fig. 6(a) and (b), respectively. The forward rate constants are rather high at temperatures of interest due to a relatively week C–H bond in the CH_2 group of phenalene and reach 8.5×10^4–4.9×10^5 s^{-1} at 1500 K depending on pressure. The higher the temperature, the more significant is an increase of the rate constant with pressure. Pressure also determines the temperature at which phenalene equilibrates with phenalenyl + H and ceases to exist as a separate chemical species; these critical temperatures were found to be 1650, 1800, 2000, 2300 and above 2500 K at 0.01, 0.1, 1, 10, and 100 atm, respectively. The reverse AP + H association reaction exhibits a high HP limit rate constant in the $4–5 \times 10^{-10}$ range owing to a high symmetry of the

Table 1
Parameters of fitted modified Arrhenius expressions $k = A^*T^{\alpha}*\exp(-E_a/RT)$ and $k = A_1{}^*T^{\alpha_1}*\exp(-E_a{}^1/RT) + A_2{}^*T^{\alpha_2}*\exp(-E_a{}^2/RT)$ for various reactions in the $C_{13}H_{10}$ and $C_{13}H_9$ systems. Pre-exponential factors A are in $cm^3\ mol^{-1}\ s^{-1}$ for bimolecular reactions and in s^{-1} for unimolecular reactions, E_a are in cal mol^{-1}.

	p, atm	A_1	α_1	$E_a{}^1$	A_2	α_2	$E_a{}^2$	T-range, K	%[a]
R → B1	0.01	$0.85316*10^{15}$	−0.42877	195.45	$-0.57324*10^{43}$	−7.8962	29,313	300–2000	10.49
	0.1	$0.29015*10^{30}$	−4.7607	10,458	$0.36509*10^{17}$	−1.0027	459.48	300–1250	1.11
		$0.41683*10^{116}$	−28.881	72,626				1250–2200	4.98
	1	$-0.24620*10^{70}$	−14.686	69,322	$0.12655*10^{15}$	−0.19452	−200.57	800–2400	2.19
	10	$0.11739*10^{21}$	−2.1022	6470.4	$0.11743*10^{16}$	−0.50381	106.07	300–1500	0.36
		$0.53428*10^{91}$	−21.224	67,597				1500–2500	5.75
	100	$0.93132*10^{15}$	−0.51373	219.11	$0.15165*10^{14}$	−0.056790	−391.43	300–1500	0.11
		$0.22855*10^{47}$	−9.0078	29,310				1500–2500	5.96
B1 → R	0.01	$0.64551*10^{65}$	−7.1235	$0.11954*10^6$	$0.12114*10^{51}$	−3.0010	$0.10940*10^6$	300–1200	2.80
		$0.41722*10^{174}$	−38.025	$0.19347*10^6$				1200–2000	2.68
	0.1	$0.14984*10^{84}$	−12.223	$0.13420*10^6$	$0.13093*10^{57}$	−4.7347	$0.11235*10^6$	500–1400	1.62
		$0.15268*10^{171}$	−36.479	$0.20113*10^6$				1400–2200	3.39
	1	$0.42366*10^{75}$	−9.6775	$0.13058*10^6$	$0.61110*10^{54}$	−3.9917	$0.11161*10^6$	500–1600	2.41
		$0.61393*10^{163}$	−33.875	$0.20642*10^6$				1600–2400	3.96
	10	$0.49939*10^{58}$	−4.8764	$0.11908*10^6$	$0.22717*10^{51}$	−2.9492	$0.11021*10^6$	500–1650	0.76
		$0.16825*10^{134}$	−25.435	$0.18758*10^6$				1650–2500	2.26
	100	$0.36128*10^{53}$	−3.4197	$0.11501*10^6$	$0.48263*10^{50}$	−2.7761	$0.10979*10^6$	500–1800	0.48
		$0.12842*10^{103}$	−16.760	$0.16359*10^6$				1800–2500	1.43
R → B2	0.01	$0.41242*10^{55}$	−11.318	41,010	$0.82990*10^{-3}$	5.1053	4825.8	500–1100	2.27
		$0.68130*10^{166}$	−43.211	$0.11215*10^6$				1100–1900	3.93
	0.1	$0.71511*10^{-3}$	5.5327	13,451	$0.16685*10^{-37}$	15.704	−6808.5	300–1000	0.73
		$0.76818*10^{88}$	−21.466	57,735	$0.31566*10^{170}$	−43.439	$0.13201*10^6$	1000–2000	5.08
	1	$0.15150*10^{17}$	−0.026738	28,928	$0.53839*10^{-25}$	11.539	−1629.2	500–1400	3.30
		$0.14042*10^{163}$	−40.680	$0.14369*10^6$				1400–2300	3.79
	10	6858.4	3.3975	24,330	$0.11535*10^{-27}$	12.084	−2075.5	500–1650	5.09
		$0.78479*10^{157}$	−38.512	$0.16082*10^6$				1650–2500	2.39
	100	$0.12817*10^{-14}$	8.4911	13,077	$0.57135*10^{-31}$	12.771	−3109.2	500–1800	4.34
		$0.50123*10^{120}$	−27.952	$0.14366*10^6$				1800–2500	2.17
B2 → R	0.01	$0.64503*10^{105}$	−18.004	$0.15644*10^6$	$0.41925*10^{37}$	1.3944	$0.11360*10^6$	500–1200	3.93
		$0.33300*10^{204}$	−46.165	$0.22194*10^6$				1200–1900	1.50
	0.1	$0.20925*10^{78}$	−9.8134	$0.14710*10^6$	$0.23148*10^{20}$	6.5513	$0.10825*10^6$	500–1300	3.97
		$0.32795*10^{205}$	−45.675	$0.23882*10^6$				1300–2000	2.01
	1	$0.22401*10^{61}$	−4.8878	$0.14169*10^6$	$0.33251*10^{13}$	8.4210	$0.10644*10^6$	500–1500	5.60
		$0.95231*10^{200}$	−43.674	$0.25372*10^6$				1500–2300	1.39
	10	$0.93297*10^{36}$	1.9692	$0.12910*10^6$	$0.26999*10^7$	10.004	$0.10456*10^6$	500–1650	4.83
		$0.39226*10^{193}$	−40.953	$0.26812*10^6$				1650–2500	2.08
	100	$0.25080*10^{21}$	6.1689	$0.12008*10^6$	1002.7	10.733	$0.10350*10^6$	500–1800	3.43
		$0.49376*10^{160}$	−31.542	$0.25552*10^6$				1800–2500	2.30
B1 → B2	0.01	$0.38657*10^{145}$	−30.401	$0.14479*10^6$				1100–1900	6.17
	0.1	$0.24695*10^{94}$	−16.279	$0.10355*10^6$	$0.42538*10^{168}$	−36.178	$0.17607*10^6$	900–2000	1.94
	1	$0.31371*10^{86}$	−13.768	$0.10186*10^6$	$0.49296*10^{158}$	−32.919	$0.17907*10^6$	1000–2300	1.39
	10	$-0.19090*10^{90}$	−13.024	$0.15137*10^6$	$0.31865*10^{29}$	2.7199	67,372	1000–2500	1.04
	100	$0.32455*10^{101}$	−16.787	$0.14049*10^6$	$0.12401*10^{52}$	−3.8141	81,018	900–2500	3.52
B2 → B1	0.01	$0.14841*10^{67}$	−8.0960	89,099	$0.59430*10^{43}$	−1.6109	70,258	500–1250	0.96
		$0.12569*10^{162}$	−34.951	$0.15473*10^6$				1250–1900	1.55
	0.1	$0.32467*10^{60}$	−6.1095	86,256	$0.96124*10^{41}$	−1.0386	69,695	500–1400	1.20
		$0.30175*10^{156}$	−32.889	$0.15938*10^6$				1400–2000	1.07
	1	$0.36581*10^{48}$	−2.6813	78,943	$0.26132*10^{39}$	−0.24481	68,734	500–1500	0.93
		$0.34975*10^{139}$	−27.790	$0.15374*10^6$				1500–2300	1.51
	10	$0.59596*10^{38}$	0.075736	70,417	$0.95098*10^{35}$	0.66658	66,846	300–1650	1.23
		$0.82078*10^{124}$	−23.407	$0.14936*10^6$				1650–2500	2.20
	100	$0.72621*10^{37}$	0.33357	69,727	$0.12032*10^{35}$	0.93725	66,556	300–1650	0.34
		$0.14403*10^{83}$	−11.920	$0.11310*10^6$				1650–2500	3.51
R → A1 + H	0.01	$0.44621*10^{122}$	−29.752	96,471	$0.20164*10^{41}$	−7.0388	34,750	800–2500	1.04
	0.1	$-0.13176*10^{107}$	−25.798	79,623	$0.14049*10^{64}$	−13.247	54,745	800–2500	6.53
	1	$0.48950*10^{-23}$	11.532	7308.3	$0.16141*10^{-42}$	16.939	−6058.3	300–1400	5.60
		$0.38406*10^{89}$	−19.757	92,706				1400–2500	5.49
	10	$0.23579*10^{-28}$	12.821	5210.7	$0.10097*10^{-43}$	16.999	−6135.4	300–1500	4.47
		$0.47329*10^{84}$	−18.128	$0.10070*10^6$				1500–2500	4.88
	100	$0.13936*10^{46}$	−7.6041	73,691	$0.23379*10^{-5}$	5.7392	17,037	800–2500	8.03
A1 + H → R	0.01	$0.28689*10^{130}$	−31.449	$0.12246*10^6$	$0.26903*10^{49}$	−8.8243	61,096	800–2500	0.67
	0.1	$0.82778*10^{88}$	−19.460	99,842				1100–2500	6.51
	1	$0.39828*10^{147}$	−37.405	$0.12616*10^6$	$0.12366*10^{100}$	−22.180	$0.12152*10^6$	1000–2500	5.97
	10	$0.26023*10^{42}$	−6.7943	69,435	$0.23365*10^{109}$	−24.322	$0.14610*10^6$	1000–2500	3.68
	100	$0.57927*10^{17}$	0.070096	55,442	$0.51303*10^{80}$	−16.398	$0.13033*10^6$	1000–2500	5.10
B1 → A1 + H	0.01	$0.16369*10^{135}$	−27.999	$0.13388*10^6$	$0.30176*10^{161}$	−34.103	$0.17340*10^6$	900–2000	3.63
	0.1	$0.10095*10^{84}$	−12.780	$0.10809*10^6$	$0.25303*10^{166}$	−34.992	$0.18794*10^6$	900–2200	3.03
	1	$0.17638*10^{138}$	−26.922	$0.17037*10^6$	$0.24117*10^{70}$	−8.8471	99,726	800–2400	5.42
	10	$0.63790*10^{113}$	−19.994	$0.15453*10^6$	$0.22835*10^{60}$	−5.8902	94,446	800–2500	4.48
	100	$0.36424*10^{81}$	−11.125	$0.12795*10^6$	$0.12887*10^{50}$	−2.8911	88,773	800–2500	3.42

(*continued on next page*)

Table 1 (*continued*)

	p, atm	A_1	α_1	$E_a{}^1$	A_2	α_2	$E_a{}^2$	*T*-range, K	%[a]
A1 + H → B1	0.01	$0.14086*10^{53}$	−11.284	19,600	$0.25063*10^{173}$	−44.542	$0.11875*10^{6}$	800–2000	3.41
	0.1	$0.15824*10^{154}$	−38.712	$0.11312*10^{6}$	$0.20844*10^{44}$	−8.6309	15,489	800–2200	6.15
	1	$0.10363*10^{137}$	−33.567	$0.10780*10^{6}$	$0.12289*10^{35}$	−5.8827	10,919	800–2400	8.14
	10	$0.76234*10^{14}$	0.054041	−5.2912	$-0.4206*10^{107}$	−23.836	$0.13420*10^{6}$	400–2500	0.25
	100	$0.19684*10^{46}$	−8.5444	31,809	$0.12649*10^{19}$	−1.2401	1682.1	500–2500	5.32
B2 → A1 + H	0.01	$0.60440*10^{68}$	−8.2265	$0.10058*10^{6}$	$0.62782*10^{46}$	−2.1630	82,344	500–1300	1.10
		$0.77368*10^{150}$	−31.333	$0.15935*10^{6}$				1300–1900	1.09
	0.1	$0.19878*10^{56}$	−4.5906	93,600	$0.28314*10^{44}$	−1.4338	81,485	500–1400	0.74
		$0.35732*10^{137}$	−27.225	0.15613*106				1400–2000	1.68
	1	$0.11630*10^{56}$	−4.4875	94,277	$0.10792*10^{44}$	−1.2870	81,430	500–1650	1.56
		$0.67192*10^{130}$	−24.960	$0.15930*10^{6}$				1650–2300	0.39
	10	$0.7534*10^{46}$	−1.9234	87,651	$0.10830*10^{41}$	−0.36645	80,272	500–1700	0.51
		$0.27338*10^{108}$	−18.581	$0.14507*10^{6}$				1700–2500	1.72
	100	$0.49488*10^{44}$	−1.3278	85,709	$0.12952*10^{40}$	−0.090775	79,886	500–1800	0.25
		$0.15513*10^{75}$	−9.4600	$0.11573*10^{6}$				1800–2500	1.19
A1 → B2 + H	0.01	$0.61941*10^{144}$	−36.617	96,890	$0.62452*10^{71}$	−16.911	29,569	800–1900	4.36
	0.1	$0.32220*10^{124}$	−30.554	88,717	$0.55339*10^{58}$	−13.005	23,264	800–2000	3.34
	1	$0.74118*10^{111}$	−26.692	86,449	$0.12860*10^{45}$	−8.9130	16,909	800–2300	5.51
	10	$0.10710*10^{82}$	−18.268	65,871	$0.23929*10^{36}$	−6.3448	12,228	800–2500	5.40
	100	$0.62488*10^{56}$	−11.286	47,379	$0.11367*10^{22}$	−2.1352	4501.2	800–2500	2.93
A1 → AP	0.01	$0.32569*10^{88}$	−14.264	$0.10091*10^{6}$	$0.18700*10^{45}$	−2.3424	68,282	500–1400	2.93
		$0.11923*10^{153}$	−32.328	$0.14992*10^{6}$				1400–1900	0.43
	0.1	$0.33744*10^{91}$	−14.857	$0.10823*10^{6}$	$0.13329*10^{40}$	−0.71566	66,551	500–1500	4.00
		$0.96042*10^{143}$	−29.366	$0.15109*10^{6}$				1500–2200	0.96
	1	$0.28721*10^{41}$	−1.1246	67,092	$0.29140*10^{74}$	−9.8056	$0.10139*10^{6}$	300–1600	4.66
		$0.23168*10^{129}$	−24.985	$0.14636*10^{6}$				1600–2400	2.15
	10	$0.62293*10^{51}$	−4.2352	71,945	$0.17062*10^{39}$	0.088548	76,209	500–1800	5.19
		$0.16420*10^{111}$	−19.751	$0.13679*10^{6}$				1800–2500	1.43
	100	$0.45645*10^{51}$	−3.9385	74,993	$0.42634*10^{96}$	−15.387	$0.13755*10^{6}$	500–2500	10.31
A1 → AP	0.1	$0.65761*10^{61}$	−6.5171	83,060				1000–2200	5.45
from dif.	1	$-0.27854*10^{159}$	−34.396	$0.15058*10^{6}$	$0.42330*10^{61}$	−6.4188	83,370	1000–2400	2.35
equations	10	$-0.40646*10^{96}$	−16.198	$0.10874*10^{6}$	$0.26357*10^{76}$	−10.493	93,439	1000–2500	5.45
	100	$-0.18001*10^{67}$	−7.9313	88,065	$0.19051*10^{57}$	−5.1071	79,873	1000–2500	6.17
AP → A1	0.01	$0.57695*10^{37}$	0.46000	88,542	$0.69403*10^{100}$	−17.436	$0.13107*10^{6}$	300–1200	0.36
		$0.82835*10^{140}$	−28.583	$0.16159*10^{6}$				1200–1900	2.52
	0.1	$0.31141*10^{78}$	−10.721	$0.12186*10^{6}$	$0.51031*10^{43}$	−1.4072	90,622	500–1400	2.89
		$0.45893*10^{137}$	−27.252	$0.16716*10^{6}$				1400–2200	2.42
	1	$0.15031*10^{41}$	−0.59266	89,885	$0.76762*10^{95}$	−15.432	$0.13950*10^{6}$	300–1500	2.23
		$0.49978*10^{132}$	−25.472	$0.17216*10^{6}$				1500–2400	3.43
	10	$0.52652*10^{46}$	−2.2150	92,957	$0.10922*10^{68}$	−7.4249	$0.12422*10^{6}$	500–1600	3.04
		$0.23433*10^{126}$	−23.363	$0.17640*10^{6}$				1600–2500	7.95
	100	$0.91707*10^{48}$	−2.7067	96,495	$0.39830*10^{109}$	−18.435	$0.17475*10^{6}$	500–2500	9.54
AP → A1	0.1	$0.33809*10^{63}$	−6.5754	$0.10698*10^{6}$				1000–2200	5.35
from dif.	1	$0.25217*10^{59}$	−5.3692	$0.10496*10^{6}$				1000–2400	7.77
equations	10	$-0.26382*10^{61}$	−6.2094	96,802	$0.32857*10^{54}$	−4.1813	92,906	1000–2500	9.52
	100	$-0.28539*10^{68}$	−7.8677	$0.11144*10^{6}$	$0.91513*10^{57}$	−4.8926	$0.10287*10^{6}$	1000–2500	6.06
AP + H → BP	0.01	$0.19043*10^{39}$	−7.1091	14,013	$0.35790*10^{18}$	−1.0545	832.96	500–1100	1.89
		$0.40919*10^{131}$	−33.520	72,075				1100–1650	1.75
	0.1	$0.46972*10^{52}$	−10.734	25,446	$0.69879*10^{22}$	−2.3415	2656.5	500–1250	0.82
		$0.17877*10^{123}$	−30.647	74,292				1250–1800	1.23
	1	$0.17348*10^{43}$	−7.9296	21,585	$0.12383*10^{20}$	−1.4690	1748.8	500–1400	0.85
		$0.36252*10^{110}$	−26.632	72,992				1400–2000	1.36
	10	$0.12043*10^{44}$	−8.0867	24,474	$0.36311*10^{18}$	−0.97649	1284.8	500–1650	1.33
		$0.85027*10^{100}$	−23.509	74,824				1650–2300	0.94
	100	$0.16399*10^{29}$	−3.8861	15,075	$0.74455*10^{16}$	−0.45236	656.59	500–1800	0.83
		$0.62634*10^{73}$	−15.810	56,967				1800–2500	0.97
BP → AP + H	0.01	$0.58462*10^{48}$	−2.7084	69,588	$0.17401*10^{40}$	−0.28485	63,143	300–1000	0.70
		$0.87464*10^{135}$	−27.891	$0.12110*10^{6}$				1000–1650	3.40
	0.1	$0.11313*10^{45}$	−1.5820	67,879	$0.10628*10^{40}$	−0.22217	63,066	300–1100	0.52
		$0.22096*10^{123}$	−23.920	$0.11836*10^{6}$				1100–1800	3.26
	1	$0.53361*10^{61}$	−6.2632	80,359	$0.70261*10^{45}$	−1.9605	65,490	500–1400	0.95
		$0.10065*10^{120}$	−22.555	$0.12348*10^{6}$				1400–2000	0.58
	10	$0.55713*10^{50}$	−3.1242	73,608	$0.61518*10^{42}$	−1.0102	64,371	500–1500	0.60
		$0.45066+*10^{102}$	−17.434	$0.11553*10^{6}$				1500–2300	0.94
	100	$0.52470*10^{46}$	−1.9741	70,799	$0.21867*10^{42}$	−0.88226	64,150	500–1700	0.45
		$0.49991*10^{86}$	−12.816	$0.10704*10^{6}$				1700–2500	0.92

[a] Maximal percentage deviation of the fitted values from the computed rate constants.

phenalenyl radical, which possesses six equivalent sites for H attachment. With rising temperature the phenomenological rate constant at finite pressures drops noticeably because of the increasing rate of the dissociation reaction, but rising pressure alleviates this decrease due to the growing collisional stabilization of phenalene.

To compute rate constants for an isolated reactive system containing $C_{13}H_{10}$, $C_{13}H_9$, and H atoms, we employed the kinetic scheme which embraces all possible elementary reactions including well-skipping channels and collisional stabilization/thermal unimolecular decomposition pathways. This means that after

solving master equations separately for the $C_{13}H_{10}$ and $C_{13}H_9$ PESs, the overall system of kinetic differential equations was solved to tie the two surfaces together and to predict concentrations of various species as functions of time. The inherent difficulty of this approach is that the eigenvalue-based master equation method fails to provide phenomenological rate constants when there is no clear separation of time scales/eigenvalues into those for the slow chemical processes (chemically significant eigenvalues, CSEs) and those for the fast energy relaxation (internal energy relaxation eigenvalues, IEREs). In order to alleviate the issue of blurring between CSEs and IEREs, the reformulated master equation approach used in the MESS package merges different isomers into one species as soon as they equilibrate on the timescale comparable to that of the energy relaxation. The species in equilibrium with each other are then united and treated as one, with the dimensionality of the effective chemical subspace also been reduced, whereas equilibration/merging between the reactive complex isomers and bimolecular reactants/products is also taken into account. The MESS package automatically merges isomers and bimolecular species at a particular temperature and pressure whenever necessary, based on the relationship between CSEs and IEREs. As a result, not all phenomenological rate constants are available from MESS calculations for $C_{13}H_{10}$ and $C_{13}H_9$ at all considered temperatures and pressures. To circumvent this deficiency, for reaction channels or temperatures/pressures where MESS could not provide phenomenological rate constants, we used their values at the HP limit or, when there were enough data to extrapolate, ones from the fitted modified Arrhenius expressions obtained from the lower-temperature rate constants. Then, the corresponding system of differential equations was solved by standard MATLAB procedures. We employed two approaches for hydrogen-elimination/attachment treatment. In the first one, the H-atoms produced on the reaction course vanished (being supposedly consumed through some other side reactions) and did not contribute to the overall hydrogen concentration [H], which was held constant. In other words, we did not solve the equation for [H]. In the second approach, variations in [H] were included. Both types of calculations lead us to the conclusion that it is impossible to reliably determine the rate constant of the overall process 1-acenaphthyl + methyl → phenalene/phenalenyl + H involving the $C_{13}H_{10}$ and $C_{13}H_9$ PESs except for a rather narrow range of parameters including temperature, pressure, and [H] in the first approach. In particular, phenomenological rate constants for two intertwined reactions cannot be determined when concentrations of the species of interest do not maintain a constant slope in their time dependence. Results of modeling which illustrate this point are presented in Supplementary Material. They made us to conclude that the rate constants derived from our RRKM-ME calculations for $C_{13}H_{10}$ and $C_{13}H_9$ should be included separately in a kinetic model and combining them in one overall reaction is not physically justified.

However, due to relatively low barriers on the $C_{13}H_9$ PES, we were able to evaluate the overall A1 ⇆ AP rate constants (shown in Fig. 5) from solving the system of kinetic differential equations, at least at temperatures above 1000–1250 K. At lower temperatures, the incubation period is too long as the times required for a slope of the concentration of the species of interest to reach a constant value are higher than 10^{-4} s. In these calculations, we took the approach in which the concentration of a reactant (A1 in the forward reaction and AP in the backward one) is set constant and the product is removed instantly, so that the reverse transformation cannot occur. The calculations corroborate that backward isomerization AP → A1 is much slower due to the difference in the barrier heights in forward and backward directions and, even at the highest temperatures, the AP → A1 rate constant is more than an order of magnitude lower than that for the forward transformation up to 2000 K (shown by solid lines in Fig. 5(a)). It is instructive to compare the A1 → AP rate constant obtained from this solution with the phenomenological values from RRKM-ME (MESS) calculations (dashed lines in Fig. 5(a)). Both sets of rate constants are close to each other at temperatures of interest, with those obtained by solving the differential equations being higher by a factor up to 5.3. The difference is attributed to the fact that the phenomenological rate constant AP → A1 from MESS takes into account only the well-skipping mechanism, whereas the differential equations also include the mechanism involving initial stabilization of an intermediate (ca. A4) followed by its thermal isomerization further to AP. All in all, this consideration corroborates the fact that A1, which is a likely product of the 1-acenaphthyl + CH_3 reaction at high temperatures, can readily isomerize to phenalenyl radical with the rate constant exhibiting a smooth Arrhenius behavior with relative weak pressure dependence.

4. Conclusions

Ab initio calculations of the $C_{13}H_{10}$ and $C_{13}H_9$ PESs related to the reaction of 1-acenaphthyl and methyl radicals and secondary isomerization of $C_{13}H_9$ radicals formed as primary reaction products were combined with RRKM-ME calculations of rate constants and relative product yields. The results indicate that the 1-acenaphthyl + CH_3 reaction proceeds by a fast radical-radical recombination mechanism and most likely produces collisionally stabilized 1-methylacenaphthalene B1 or a $C_{13}H_9$ benzylic radical A1 after an H loss from the CH_3 group. Both reaction channels are predicted to be exothermic, by 106.8 and 25.2 kcal/mol, respectively. The A1 + H channel is preferable at higher temperatures, whereas the stabilization of 1-methylacenaphthalene is favored at higher pressures. The radical A1 can interconvert to phenalenyl radical AP via an isomerization process involving formal insertion of the CH_2 group into a C–C bond of the five-member ring leading to expansion of this ring to a six-member ring. The A1 → AP isomerization is calculated to be 22.7 kcal/mol exothermic and is predicted to be nearly irreversible up to 2000 K. The H addition reaction to phenalenyl radical to form phenalene and the reverse H loss from phenalene were also considered and the weakest C–H bond in the CH_2 group of phenalene is computed to be only 62.2 kcal/mol strong, weaker than typical benzylic bonds, 88.5 and 81.6 kcal/mol in toluene [26] and 1-methylacenaphthalene B1, respectively. The analysis of the reaction kinetics allowed us to deduce the following mechanism for the conversion of 1-acenaphthyl radical to phenalene or phenalenyl radical + H via methylation:

$$\text{1-acenaphthyl} + CH_3 \leftrightarrows \text{A1} + \text{H}$$

$$\rightarrow \text{B1/B2}$$

$$\text{B1} \leftrightarrows \text{B2}$$

$$\text{B1/B2} \leftrightarrows \text{A1} + \text{H}$$

$$\text{A1} \leftrightarrows \text{AP}$$

$$\text{AP} + \text{H} \leftrightarrows \text{BP}$$

It should be noted that the benzylic radical A1 can be also obtained from 1-methylacenaphthalene B1 by intermolecular H abstraction from the CH_3 group. Rate constants for the significant elementary reactions are fitted to modified Arrhenius expressions or sums of two modified Arrhenius expressions where necessary and are assembled in Table 1. These rate constants are recommended for kinetic modeling of the expansion of a five-member ring on a zigzag edge of a PAH to a six-member ring to form a phenalene-like structure or a resonantly stabilized phenalenyl-like radical. It

should be noted however that the overall rate constant for the $C_{12}H_7 + CH_3$ reaction is controlled by that for the barrierless entrance channel and hence is contingent on the rate constant for the reaction between phenyl and methyl radicals. Therefore, the rate constants generated here can be subjected to further study and be updated if prospective works explicitly determine the rate constants for the reaction between acenaphthyl and methyl radicals.

While the acenaphthyl $+ CH_3$ reaction and the coupled secondary reactions of the $C_{13}H_9$ radicals provide a viable pathway to phenalenyl radical and phenalene, further studies are needed to evaluate their ultimate contribution into the formation of these species and their further role in the PAH growth. Other alternative reactions need to be investigated such as, for example, the reactions of 1-naphthyl with C_3H_4 isomers (and possibly with C_3H_5 and C_3H_6) and methyl addition to acenaphthenyl $C_{12}H_9$ obtained by H abstraction from acenaphthene $C_{12}H_{10}$ followed by H_2/2H loss to produce the $C_{13}H_{10}$ isomers. To make a conclusion which of the alternative mechanisms is the most important, one needs to generate (or measure) rate constants for a variety of possible mechanisms and then compare their contributions via kinetic modeling.

Declaration of Competing Interest

The authors declare that they have no known competing financial interests or personal relationships that could have appeared to influence the work reported in this paper.

Acknowledgments

The work was supported by the Ministry of Science and Higher Education of the Russian Federation via the grant No. 14.Y26.31.0020. The work at FIU was funded by the U.S. Department of Energy, Basic Energy Sciences, grant DE-FG02-04ER15570.

Supplementary materials

Supplementary material associated with this article can be found, in the online version, at doi:10.1016/j.combustflame.2019.11.038.

References

[1] M. Frenklach, Reaction mechanism of soot formation in flames, Phys. Chem. Chem. Phys. 4 (2002) 2028–2037.
[2] P. Lindstedt, L. Maurice, M. Meyer, Thermodynamic and kinetic issues in the formation and oxidation of aromatic species, Faraday Discuss. 119 (2002) 409–432.
[3] M.J. Castaldi, N.M. Marinov, C.F. Melius, J. Hwang, S.M. Senkan, W.J. Pitz, C.K. Westbrook, Experimental and modeling investigation of aromatic and polycyclic aromatic hydrocarbon formation in a premixed ethylene flame, Symp. (Int.) Combust. 26 (1996) 693–702.
[4] N.M. Marinov, W.J. Pitz, C.K. Westbrook, M.J. Castaldi, S.M. Senkan, Modeling of aromatic and polycyclic aromatic hydrocarbon formation in premixed methane and ethane flames, Combust. Sci. Technol. 116/117 (1996) 211–287.
[5] H. Richter, W.J. Grieco, J.B. Howard, Formation mechanism of polycyclic aromatic hydrocarbons and fullerenes in premixed benzene flames, Combust. Flame 119 (1999) 1–22.
[6] N.M. Marinov, W.J. Pitz, C.K. Westbrook, A.M. Vincitore, M.J. Castaldi, S.M. Senkan, C.F. Melius, Aromatic and polycyclic aromatic hydrocarbon formation in a laminar premixed n-butane flame, Combust. Flame 114 (1998) 192–213.
[7] S. Granata, T. Faravelli, E. Ranzi, N. Olten, S.M. Senkan, Kinetic modeling of counterflow diffusion flames of butadiene, Combust. Flame 131 (2002) 273–284.
[8] M. Frenklach, H. Wang, Detailed modeling of soot particle nucleation and growth, Symp. (Int.) Combust. 23 (1991) 1559–1566.
[9] V.V. Kislov, N.I. Islamova, A.M. Kolker, S.H. Lin, A.M. Mebel, Hydrogen abstraction acetylene addition and Diels-Alder mechanisms of PAH formation: a detailed study using first principles calculations, J. Chem. Theory and Comput. 1 (2005) 908–924.
[10] J. Cioslowski, M. Schimeczek, P. Piskorz, D. Moncrieff, Thermal rearrangement of ethynylarenes to cyclopentafused polycyclic aromatic hydrocarbons: an electronic structure study, J. Am. Chem. Soc. 121 (1999) 3773–3778.
[11] M. Frenklach, D.W. Clary, W.C. Gardiner, S.E. Stein, Detailed kinetic modeling of soot formation on shock-tube pyrolysis of acetylene, Symp. (Int.) Combust. 20 (1984) 887–901.
[12] J.A. Miller, Theory and modeling in combustion chemistry, Symp. (Int.) Combust. 26 (1996) 461–480.
[13] A.T. Ciajolo, M. Mallardo, T. Faravelli, E. Ranzi, Experimental and kinetic modeling study of sooting atmospheric-pressure cyclohexane flame, Proc. Combust. Inst. 32 (2009) 585–591.
[14] N. Hansen, J.A. Miller, T. Kasper, K. Kohse-Hoinghaus, P.R. Westmoreland, J. Wang, T.A. Cool, Benzene formation in premixed fuel-rich 1,3-butadiene flames, Proc. Combust. Inst. 32 (2009) 623–630.
[15] C. Marchal, J.L. Delfau, C. Vovelle, G. Moreac, C. Mounaim-Rousselle, F. Mauss, Modelling of aromatics and soot formation from large fuel molecules, Proc. Combust. Inst. 32 (2009) 753–759.
[16] H. Wang, M. Frenklach, A detailed kinetic modeling study of aromatics formation in laminar premixed acetylene and ethylene flames, Combust. Flame 110 (1997) 173–221.
[17] J. Appel, H. Bockhorn, M. Frenklach, Kinetic modeling of soot formation with detailed chemistry and physics: laminar premixed flames of C-2 hydrocarbons, Combust. Flame 121 (2000) 122–136.
[18] A. D'Anna, A. Violi, A. D'Allesio, Modeling the rich combustion of aliphatic hydrocarbons, Combust. Flame 121 (2000) 418–429.
[19] D'Anna, A. Violi, A kinetic model for the formation of aromatic hydrocarbons in premixed laminar flames, Symp. (Int.) Combust. 27 (1998) 425–433.
[20] P. Lindstedt, Modeling of the chemical complexities of flames, Symp. (Int.) Combust. 27 (1998) 269–285.
[21] J.A. Miller, Concluding remarks, Faraday Discuss. 119 (2001) 461–475.
[22] C. Saggese, S. Ferrario, J. Camacho, A. Cuoci, A. Frassoldati, E. Ranzi, H. Wang, T. Faravelli, Kinetic modeling of particle size distribution of soot in a premixed burner-stabilized stagnation ethylene flame, Combust. Flame 162 (2015) 3356–3369.
[23] V.V. Kislov, A.I. Sadovnikov, A.M. Mebel, Formation mechanism of polycyclic aromatic hydrocarbons beyond the second aromatic ring, J. Phys. Chem. A 117 (2013) 4794–4816.
[24] D.S.N. Parker, R.I. Kaiser, B. Bandyopadhyay, O. Kostko, T.P. Troy, M. Ahmed, Unexpected chemistry from the reaction of naphthyl and acetylene at combustion-like temperatures, Angew. Chem. Int. Ed. 54 (2015) 5421–5424.
[25] A.M. Mebel, Y. Georgievskii, A.W. Jasper, S.J. Klippenstein, Temperature- and pressure-dependent rate coefficients for the HACA pathways from benzene to naphthalene, Proc. Combust. Inst. 36 (2017) 919–926.
[26] A.M. Mebel, Y. Georgievskii, A.W. Jasper, S.J. Klippenstein, Pressure-dependent rate constants for PAH growth: formation of indene and its conversion to naphthalene, Faraday Discuss. 195 (2016) 637–670.
[27] A.M. Mebel, A. Landera, R.I. Kaiser, Formation mechanisms of naphthalene and indene: from the interstellar medium to combustion flames, J. Phys. Chem. A 121 (2017) 901–926.
[28] R.I. Singh, A.M. Mebel, M. Frenklach, Oxidation of graphene-edge six- and five-member rings by molecular oxygen, J. Phys. Chem. A 119 (2015) 7528–7547.
[29] M. Frenklach, Z. Liu, R.I. Singh, G.R. Galimova, V.N. Azyazov, A.M. Mebel, Detailed, sterically-resolved modeling of soot oxidation: role of o atoms, interplay with particle nanostructure, and emergence of inner particle burning, Combust. Flame 188 (2018) 284–306.
[30] F. Schulz, M. Commodo, K. Kaiser, G. De Falco, P. Minutolo, G. Meyer, A. D'Anna, L. Gross, Insights into incipient soot formation by atomic force microscopy, Proc. Combust. Inst. 37 (2018) 885–892.
[31] C.F. Melius, M.E. Colvin, N.M. Marinov, W.J. Pitz, S.M. Senkan, Reaction mechanisms in aromatic hydrocarbon formation involving the C_5H_5 cyclopentadienyl moiety, Symp. (Int.) Combust. 26 (1996) 685–692.
[32] L.V. Moskaleva, A.M. Mebel, M.C. Lin, The $CH_3 + C_5H_5$ reaction: a potential source of benzene at high temperatures, Symp. (Int.) Combust. 26 (1996) 521–526.
[33] S. Sharma, W.H. Green, Computed rate coefficients and product yields for c-$C_5H_5 + CH_3$ products, J. Phys. Chem. A 113 (2009) 8871–8882.
[34] A.W. Jasper, N. Hansen, Hydrogen-assisted isomerizations of fulvene to benzene and of larger cyclic aromatic hydrocarbons, Proc. Combust. Inst. 34 (2013) 279–287.
[35] L. Zhao, R.I. Kaiser, W. Lu, B. Xu, M. Ahmed, A.N. Morozov, A.M. Mebel, A.H. Howlader, S.F. Wnuk, Molecular mass growth through ring expansion in polycyclic aromatic hydrocarbons via radical-radical reactions, Nat. Commun. 10 (2019) 3689.
[36] M. Frenklach, T. Yuan, M.K. Ramachandra, Soot formation in binary hydrocarbon mixtures, Energy Fuels 2 (1988) 462–480.
[37] B. Shukla, A. Miyoshi, M. Koshi, Role of methyl radicals in the growth of PAHs, J. Am. Soc. Mass Spectrom. 21 (2010) 534–544.
[38] K.O. Johansson, M.P. Head-Gordon, P.E. Schrader, K.R. Wilson, H.A. Michelsen, Resonance-stabilized hydrocarbon-radical chain reactions may explain soot inception and growth, Science 361 (2018) 997–1000.
[39] S.V. Kalpathy, N.B. Poddar, S.P. Bagley, M.J. Wornat, Reaction pathways for the growth of polycyclic aromatic hydrocarbons during the supercritical pyrolysis of n-decane, as determined from doping experiments with 1- and 2-methylnaphthalene, Proc. Combust. Inst. 35 (2015) 1833–1841.
[40] E.A. Hurst, N.B. Poddar, K. Vutukuru, S.V. Kalpathy, M.J. Wornat, Polycyclic aromatic hydrocarbons formation and growth during the supercritical pyrolysis of 1-octene, Proc. Combust. Inst. 37 (2019) 1107–1115.

[41] A.D. Becke, Density-functional thermochemistry. III. The role of exact exchange, J. Chem. Phys. 98 (1993) 5648–5652.
[42] C. Lee, W. Yang, R.G. Parr, Development of the Colle-Salvetti correlation-energy formula into a functional of the electron density, Phys. Rev. B 37 (1988) 785–789.
[43] M.J. Frisch, G.W. Trucks, H.B. Schlegel, G.E. Scuseria, M.A. Robb, J.R. Cheeseman, G. Scalmani, V. Barone, B. Mennucci, G.A. Petersson, et al., Gaussian 09, Revision D.01, Gaussian, Inc., Wallingford, CT, 2009.
[44] A.G. Baboul, L.A. Curtiss, P.C. Redfern, K. Raghavachari, Gaussian-3 theory using density functional geometries and zero-point energies, J. Chem. Phys. 110 (1999) 7650–7657.
[45] L.A. Curtiss, K. Raghavachari, P.C. Redfern, A.G. Baboul, J.A. Pople, Gaussian-3 theory using coupled cluster energies, Chem. Phys. Lett. 314 (1999) 101–107.
[46] J.A. Miller, M.J. Pilling, J. Troe, Unravelling combustion mechanisms through a quantitative understanding of elementary reactions, Proc. Combust. Inst. 30 (2005) 43–88.
[47] A. Fernandez-Ramos, J.A. Miller, S.J. Klippenstein, D.G. Truhlar, Modeling the kinetics of bimolecular reactions, Chem. Rev. 106 (2006) 4518–4584.
[48] D.G. Truhlar, B.C. Garrett, S.J. Klippenstein, Current status of transition-state theory, J. Phys. Chem. 100 (1996) 12771–12800.
[49] Y. Georgievskii, J.A. Miller, M.P. Burke, S.J. Klippenstein, Reformulation and solution of the master equation for multiple-well chemical reactions, J. Phys. Chem. A 117 (2013) 12146–12154.
[50] Y. Georgievskii, S.J. Klippenstein, Master equation system solver (MESS), 2015, available online at https://github.com/PACChem/MESS.
[51] H. Wang, M. Frenklach, Transport properties of polycyclic aromatic hydrocarbons for flame modeling, Combust. Flame 96 (1994) 163–170.
[52] A. Vishnyakov, P.G. Debenedetti, A.V. Neimark, Statistical geometry of cavities in a metastable confined fluid, Phys. Rev. E 62 (2000) 538–544.
[53] A.V. Neimark, P.I. Ravikovitch, A. Vishnyakov, Adsorption hysteresis in nanopores, Phys. Rev. E 62 (2000) 1493–1496.
[54] J. Troe, Theory of thermal unimolecular reactions at low pressures. I. Solutions of the master equation, J. Chem. Phys. 66 (1977) 4745–4757.
[55] A.W. Jasper, C.M. Oana, J.A. Miller, Third-body collision efficiencies from combustion modeling: hydrocarbons in atomic and diatomic baths, Proc. Combust. Inst. 35 (2015) 197–204.
[56] M. Frenklach, R.I. Singh, A.M. Mebel, On the low-temperature limit of HACA, Proc. Combust. Inst. 37 (2019) 969–976.
[57] S.J. Klippenstein, J.I. Cline, Classical phase space theory for product state distributions with application to the v–j vector correlation, J. Chem. Phys. 103 (1995) 5451–5460.
[58] S.J. Klippenstein, L.B. Harding, Y. Georgievskii, On the formation and decomposition of C_7H_8, Proc. Combust. Inst. 31 (2007) 221–229.
[59] L.B. Harding, S.J. Klippenstein, Y. Georgievskii, On the combination reactions of hydrogen atoms with resonance-stabilized hydrocarbon radicals, J. Phys. Chem. A 111 (2007) 3789–3801.
[60] J.M. Zoellner, R.W. Zoellner, The isomers of phenalene and their singlet and triplet states: a Hartree-Fock and density functional computational investigation, J. Mol. Struct. (THEOCHEM) 863 (2008) 50–54.